

Terbium-Doped VO₂ Thin Films: Reduced Phase Transition Temperature and Largely Enhanced Luminous Transmittance

Wang, Ning; Duchamp, Martial; Dunin-Borkowski, Rafal E.; Liu, Shiyu; Zeng, Xianting; Cao, Xun; Long, Yi

2016

Wang, N., Duchamp, M., Dunin-Borkowski, R. E., Liu, S., Zeng, X., Cao, X., et al. (2016). Terbium-Doped VO₂ Thin Films: Reduced Phase Transition Temperature and Largely Enhanced Luminous Transmittance. *Langmuir*, 32(3), 759-764.

<https://hdl.handle.net/10356/84947>

<https://doi.org/10.1021/acs.langmuir.5b04212>

© 2016 American Chemical Society. This is the author created version of a work that has been peer reviewed and accepted for publication by *Langmuir*, American Chemical Society. It incorporates referee's comments but changes resulting from the publishing process, such as copyediting, structural formatting, may not be reflected in this document. The published version is available at: [<http://dx.doi.org/10.1021/acs.langmuir.5b04212>].

Downloaded on 24 Aug 2022 16:16:15 SGT

Terbium-Doped VO₂ Thin Films: Reduced Phase Transition Temperature and Largely Enhanced Luminous Transmittance

Ning Wang, Martial Duchamp, Rafal E. Dunin-Borkowski, Shiyu Liu, Xianting Zeng, Xun Cao, and Yi Long

Langmuir, **Just Accepted Manuscript** • DOI: 10.1021/acs.langmuir.5b04212 • Publication Date (Web): 04 Jan 2016

Downloaded from <http://pubs.acs.org> on January 5, 2016

Just Accepted

“Just Accepted” manuscripts have been peer-reviewed and accepted for publication. They are posted online prior to technical editing, formatting for publication and author proofing. The American Chemical Society provides “Just Accepted” as a free service to the research community to expedite the dissemination of scientific material as soon as possible after acceptance. “Just Accepted” manuscripts appear in full in PDF format accompanied by an HTML abstract. “Just Accepted” manuscripts have been fully peer reviewed, but should not be considered the official version of record. They are accessible to all readers and citable by the Digital Object Identifier (DOI®). “Just Accepted” is an optional service offered to authors. Therefore, the “Just Accepted” Web site may not include all articles that will be published in the journal. After a manuscript is technically edited and formatted, it will be removed from the “Just Accepted” Web site and published as an ASAP article. Note that technical editing may introduce minor changes to the manuscript text and/or graphics which could affect content, and all legal disclaimers and ethical guidelines that apply to the journal pertain. ACS cannot be held responsible for errors or consequences arising from the use of information contained in these “Just Accepted” manuscripts.



1
2
3 Terbium-Doped VO₂ Thin Films: Reduced Phase Transition Temperature and Largely Enhanced
4
5
6 Luminous Transmittance
7

8
9 Ning Wang,^a Martial Duchamp,^b Rafal E Dunin-Borkowski,^b Shiyu Liu,^c XianTing Zeng,^c Xun
10
11 Cao,^a and Yi Long^{a*}
12

13
14 Address:
15

16
17
18 ^a School of Materials Science and Engineering, Nanyang Technological University, 50 Nanyang
19
20 Avenue, (Singapore) 639798
21

22
23 ^b Ernst Ruska-Centre for Microscopy and Spectroscopy with Electrons (ER-C) and Peter
24
25 Grünberg Institute (PGI), Forschungszentrum Jülich, 52428 Jülich, Germany
26
27

28
29 ^c Singapore Institute of Manufacturing Technology, 71 Nanyang Drive, 638075 Singapore
30
31

32
33 * Corresponding author: Dr Long Yi, E-mail: longyi@ntu.edu.sg
34
35
36
37
38
39
40
41
42
43
44
45
46
47
48
49
50
51
52
53
54
55
56
57
58
59
60

1
2
3 Abstract. Vanadium dioxide (VO_2) is a well-known thermochromic material with large IR
4 modulating ability, promising for energy saving smart windows. The main drawbacks of VO_2 are
5 its high phase transition temperature ($\tau_c = 68\text{ }^\circ\text{C}$), low luminous transmission (T_{lum}) and weak
6 solar modulating ability (ΔT_{sol}). In this paper, the terbium cation (Tb^{3+}) doping was firstly
7 reported to reduce τ_c and increase T_{lum} of VO_2 thin films. Compared with pristine VO_2 , 2 at.%
8 doping level gives both enhanced T_{lum} and ΔT_{sol} from 45.8% to 54.0% and 7.7% to 8.3%,
9 respectively. The T_{lum} increases with continuous Tb^{3+} doping, and reaches 79.4% at 6 at.%
10 doping level, representing $\sim 73.4\%$ relative increment compared with pure VO_2 . This has
11 surpassed the best reported doped VO_2 thin films. The enhanced thermochromic properties is
12 meaningful for smart window applications of VO_2 materials.
13
14
15
16
17
18
19
20
21
22
23
24
25
26
27
28
29
30

31 Keywords: Vanadium dioxide; Terbium-doping; Thermochromic properties; Sol-gel; Smart
32 windows
33
34
35
36
37
38
39

40 1. Introduction

41
42 Vanadium dioxide (VO_2) is a well-studied thermochromic material that undergoes fully
43 reversible metal-insulator transitions (MIT). At the critical temperature (τ_c) of $68\text{ }^\circ\text{C}$,^{1, 2} VO_2
44 transforms from semiconducting monoclinic phase to metallic rutile phase, which can be
45 reflected by a sharp change in infrared (IR) transmittance while visible light transmittance (T_{lum})
46 stays nearly constant. As its τ_c being the closest to the room temperature amongst transition metal
47 oxides, while taking the advantage of being transparent at both states (hot metallic and cool
48 insulating states) compared to the newly developed organic³ and hybrid⁴ smart systems based on
49
50
51
52
53
54
55
56
57
58
59
60

temperature-responsive hydrogel matrices, VO₂ has since become the most potential choice to be applied in energy-saving smart windows⁵⁻⁷ and other thermal/optical/sensing devices.⁸⁻¹²

VO₂ faces the drawback of both low T_{lum} and solar modulating ability (ΔT_{sol} , the ability to regulate the input solar energy). Simultaneously enhancing these properties has been achieved through casting VO₂ nanoparticles/matrix composite foils,^{13, 14} thin film nanostructuring such as bio-inspired VO₂ with anti-reflection (AR) effects¹⁵ and controlled nanoporosity¹⁶. By far, high τ_c is the most crucial issue that hinders the application of thermochromic smart windows, and the most efficient way to reduce τ_c is doping, although some dopants may degrade T_{lum} . **Table 1** lists the selected dopants which can reduce τ_c . It is of interest to observe that most dopants have a certain upper limit in doping level to reduce τ_c . The reducing rate and the effects on T_{lum} is also summarized in this table.

Table 1 Effects of selected dopants on τ_c and T_{lum} of VO₂

Dopant	Limit	Effect on τ_c	Effect on T_{lum}
Eu ³⁺ ¹⁷	4 at.%	-6.5 °C/at.%	Increased by 22% at 4 at.%
Mg ²⁺ ¹⁸⁻²⁰	7 at.%	-3 °C/at.%	Increased by 11% at 7 at.%
W ⁶⁺ ²¹	2.5 at.%	-23 °C/at.%	Decreased by 10% at 2.5 at.%
F ⁻ ²¹	2.1 at.%	-20 °C/at.%	unchanged
Mo ⁶⁺ ²²	2.5 at.%	-12 °C/at.%	Decreased by 10% at 3 at.%
Nb ⁵⁺ ²²	4 at.%	-8 °C/at.%	Decreased by 50% at 11 at.%
P ³⁻ ²³	1 at.%	-13 °C/at.%	Not available
Fe ³⁺ ²⁴	1.4 at.%	-6 °C/at.%	Not available
Sb ³⁺ ²⁵	7 at.%	-1 °C/at.%	35% at 3 at.%. Increased by 65%
Zr ⁴⁺ ²⁶	11 at.%	unchanged.	Increased by 65%

1
2
3
4
5
6
7
8
9
10
11
12
13
14
15
16
17
18
19
20
21
22
23
24
25
26
27
28
29
30
31
32
33
34
35
36
37
38
39
40
41
42
43
44
45
46
47
48
49
50
51
52
53
54
55
56
57
58
59
60

Rare earth ions (RE^{3+}) have large ionic radii and rich valence shell electrons. Therefore, doping RE^{3+} into VO_2 crystal lattice could lead to appreciable extra strain energy via structure deformation and altered holes or electrons carrier density which may profit enhancing the thermochromic properties of VO_2 .²⁷ In this work, we firstly report the Tb^{3+} doping in VO_2 lattice, and its effect on lowering down the τ_c and significantly increasing the T_{lum} has been investigated systematically.

2. Experimental section

The chemicals used in this study were vanadium (V) oxide (V_2O_5 , 99.99%, Alfa Aesar), terbium oxide (Tb_2O_3 , 99.99%, Alfa Aesar), hydrogen peroxide (H_2O_2 , 30 wt%, VWR) and polyvinylpyrrolidone (PVP, 99%, Sigma-Aldrich). All of the chemicals were used as received without any further purification.

2.1 Synthesis of Tb-doped VO_2 (M) thin films

180 mg of V_2O_5 powder and required amount of Tb_2O_3 powder were added into 15 mL of H_2O_2 at 70 °C. After 10 minutes of stirring at 800 rpm, a vigorous exothermic reaction took place and formed a reddish-brown sol. The precursor was then cooled in an ice bath and another 1 mL of H_2O_2 was added to dissolve any remaining Tb_2O_3 powder. 12 mg of PVP was subsequently added to improve the viscosity of the precursor, which was dip-coated onto a $15 \times 15 \times 0.5 \text{ mm}^3$ pre-cleaned fused silica substrate using a dip coater (KSV Instruments) at a speed of 300 mm/min. The precursor film was annealed at 550 °C for 2 h in a tube furnace with argon (99.9995%, NOX) atmosphere, during which the ramping rate was set to 1.0 °C/min, and gas flow rate was tuned to ~200 mL/min.

2.2 Characterization

The phases of the samples were determined with an XRD-6000 X-ray diffractometer (XRD, Shimadzu, Japan), of which the Cu-K α radiation was produced at 40 kV and 30 mA with $\lambda \approx 0.15406$ nm at an X-ray grazing angle of 1.0°. The surface morphology, roughness and particle size analyses were examined using a Digital Instrument DI3100 atomic force microscope (AFM, Bruker, Germany) under tapping mode. The Transmission Electron Microscope (TEM) characterization was performed with JEOL JEM-2010 with the accelerating voltage of 200 kV. The XPS data were collected in the V 2p and Tb 3d binding energy regions using a Thermo Scientific ESCALAB 250Xi XPS spectrometer (900 μ m spot, 3 scans, 75 eV pass energy) equipped with Avantage Data System software. The transmittance spectra and hysteresis loop were collected using a Cary 5000 ultraviolet-visible light-near infrared (UV-Vis-NIR) spectrophotometer (Agilent, USA), which was equipped with a PE120 peltier system simple heating and cooling stage (Linkam, UK). The calculations of integrated T_{lum} ($380 \leq \lambda \leq 780$ nm) and ΔT_{sol} ($280 \leq \lambda \leq 2500$ nm) can be found in equations (1) and (2) respectively.

$$T_{lum/sol} = \int \varphi_{lum/sol}(\lambda) T(\lambda) d\lambda / \int \varphi_{lum/sol}(\lambda) d\lambda \quad (1)$$

$$\Delta T_{sol} = T_{sol}(20 \text{ }^\circ\text{C}) - T_{sol}(90 \text{ }^\circ\text{C}) \quad (2)$$

Where $T(\lambda, \tau)$ is the recorded percentage transmittance at a particular wavelength and temperature, φ_{lum} is the standard luminous efficiency function for the photopic vision of human eyes,²⁸ and φ_{sol} is the solar irradiance spectrum for air mass 1.5 (corresponding to the Sun standing 37° above the horizon).²⁹

3. Results and discussion

3.1 Synthesis of Tb doped VO₂ thin films

Figure 1a shows the XRD patterns of the Tb doped VO₂ thin films. As depicted, all of the samples (V_{1-x}Tb_xO₂, x=0-10 at.%) exhibit the characteristic (011) peak at $2\theta = \sim 28^\circ$, revealing the formation of VO₂(M) phase (JCPDS #82-661). In addition, no other vanadium oxide phase peaks can be found in the patterns, which proves the high phase purity of the VO₂ thin films. The high resolution XPS scan of V2p and Tb3d was performed in the binding energy range of 535-507 eV and 1287-1235 eV, respectively. As shown in Figure 1b, the V2p_{3/2} peak can be split into two peaks located at 518.6 and 517.8 eV, which should be ascribed to the V⁵⁺ and V⁴⁺, respectively. The existence of V⁵⁺ should be attributed to the partial oxidation of the thin film within several nanometers scale in the top layer. The Tb3d peaks can be clearly observed in Figure 1c, and the Tb3d_{3/2} and Tb3d_{5/2} peaks locate at 1278.4 and 1243.4 eV, respectively. The calculated doping level of Tb³⁺ based on the XPS spectra of V2p and Tb3d is ~ 10.3 at.%, in accordance with the stoichiometry of the sample V_{0.9}Tb_{0.1}O₂.

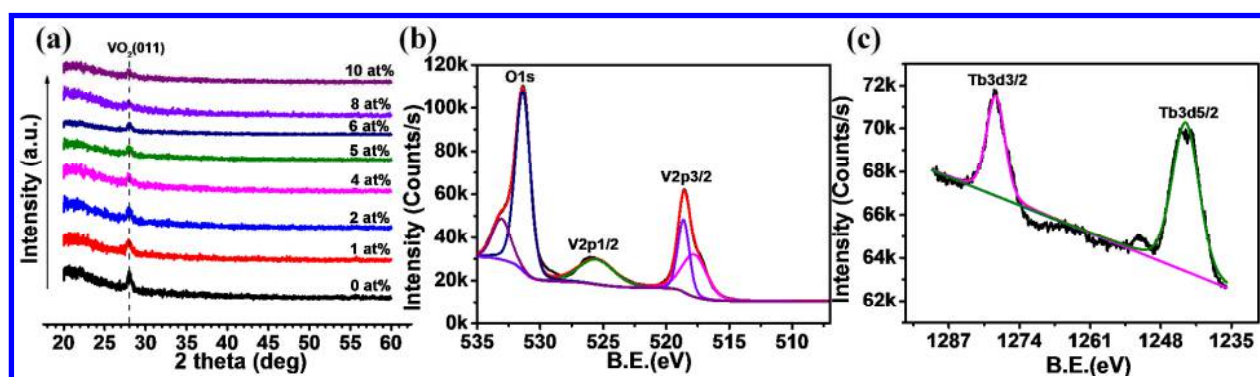


Figure 1. XRD patterns of Tb-doped VO₂ thin films (a); High resolution XPS scan of V2p (b) and Tb3d (c) for the sample V_{0.9}Tb_{0.1}O₂.

1
2
3 The morphology of the thin films is shown in Figure 2 and the mean particle size analysed with
4 NanoScope Analysis 3.0 software ranges approximately from 50 nm to 80 nm, with the
5
6 exception of ~ 100 nm at 10 at.% Tb doping (Table 2). The measured roughness value ranges
7
8 from 0.7 to 4.5 nm, and the smoothness would indicate an even distribution of the VO₂
9
10 nanoparticles on the fused silica substrates as shown in the 2D images, which may lead to the
11
12 high average T_{lum} of the samples. The morphology and the phase of VO₂ thin film has been
13
14 further confirmed by the TEM characterization. As shown in Figure 3, the thin film
15
16 (V_{0.98}Tb_{0.02}O₂) exhibits the average grain size ~62 nm (Figure 3a), in accordance with the AFM
17
18 result. The pattern of Selected Area Electron Diffraction (SAED, Figure 3b) can be indexed with
19
20 VO₂ crystalline faces (011), (-211), (-212) and (220). The Tb doping was further confirmed by
21
22 the HRTEM as shown in Figure 3c, where the larger Tb atoms (pointed by black arrows) could
23
24 be observed in the lattice distortion region arising from the replacement of V by Tb [ionic radius
25
26 ratio: 0.92 Å (Tb³⁺) v.s. 0.58 Å (V⁴⁺)]. The EDX mapping, as shown in Figure 3d and e, reveals
27
28 the uniform doping of Tb in the VO₂ thin film.
29
30
31
32
33
34
35
36
37
38
39
40
41
42
43
44
45
46
47
48
49
50
51
52
53
54
55
56
57
58
59
60

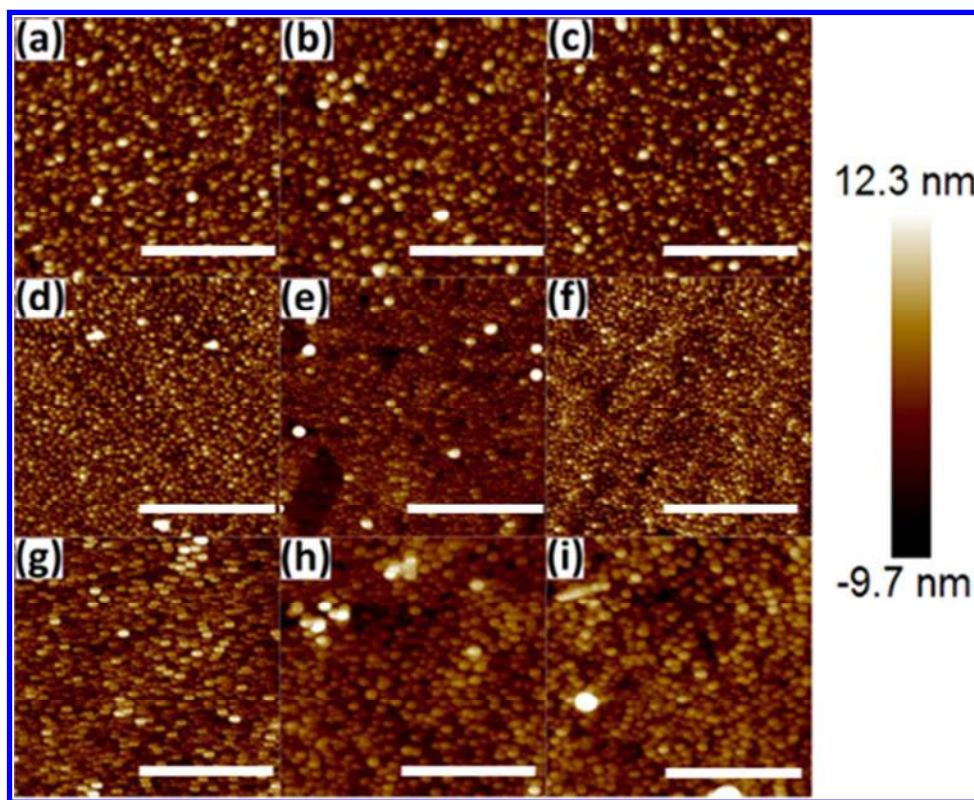


Figure 2. 2D AFM images in height of (a-g) 0-6 at.%; (h) 8 at.% and (i) 10 at.% Tb-doped VO_2 thin films. The scan area of each image is $2 \times 2 \mu\text{m}^2$ and all of the scale bars represent $1 \mu\text{m}$.

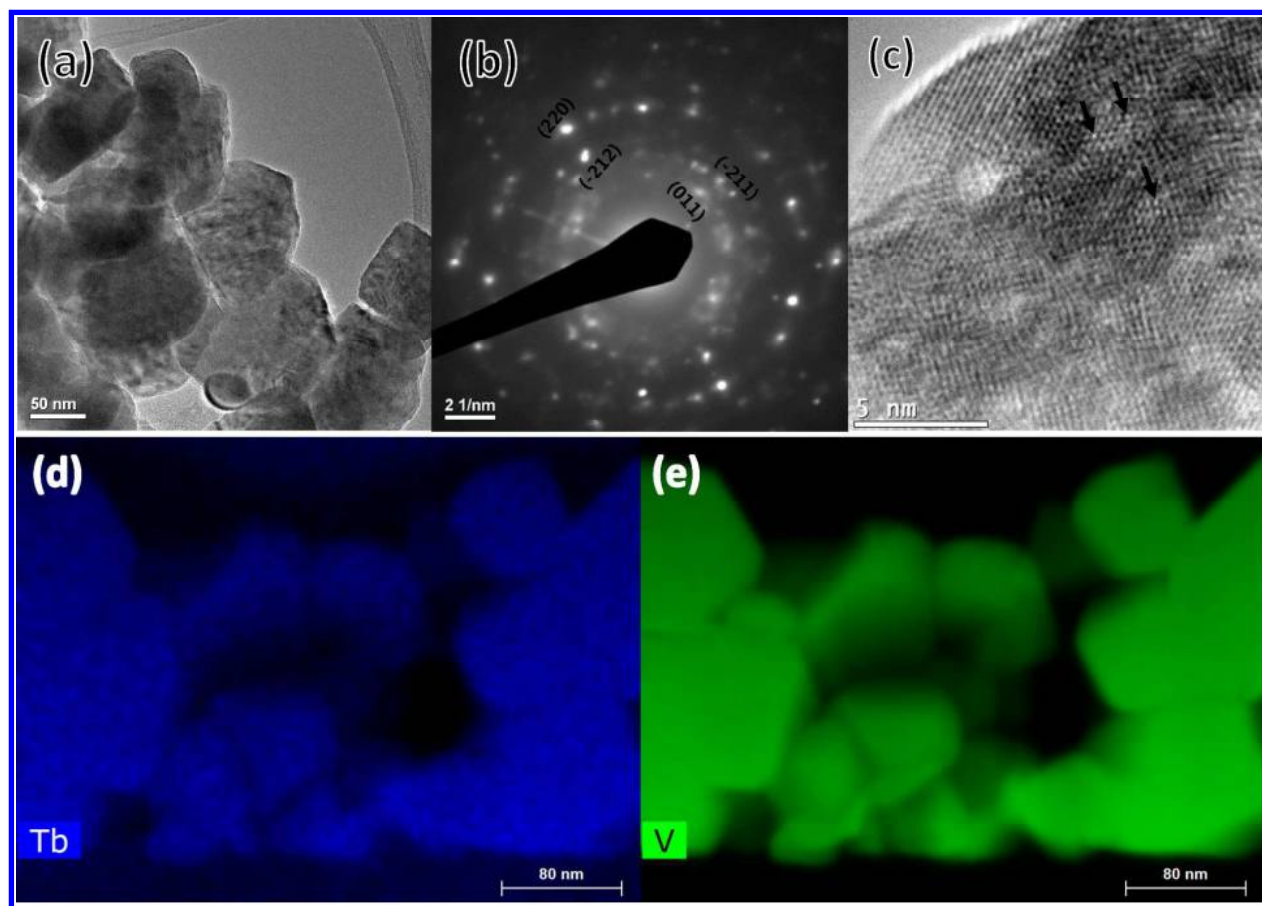


Figure 3. TEM image (a), SAED pattern (b) and the HRTEM (c) for the sample $V_{0.98}Tb_{0.02}O_2$.

(d) and (e) are the EDX mapping of Tb, V elements, respectively.

3.2 Thermochromic properties

Figure 4a displays the UV-Vis-NIR spectra of the samples. It can be observed that as Tb doping level increases, the average T_{lum} is continuously improved from 45.8% (undoped) and capped at 79.0% (6 at.% Tb-doped), after which falling back slightly (Figure 4b/Table 2). Tb doping largely enhances the transmission in both visible and infrared (IR) range at both high and low temperatures. With higher Tb doping level, transmittance contrast at $\lambda = 2500$ nm gets smaller, possibly due to the adjustment in crystal structure as a result of introduction of large Tb^{3+} dopant

ions. The interference effect between the %T at low and high temperatures¹⁶ is observed from 0 to 2 at.% Tb doping, where the crossing points of temperature dependent %T curves show a blue-shift trends along with the RE doping. This could lead to the slight enhancement in ΔT_{sol} from 7.7% to 8.3%. However, when Tb doping level is beyond 2 at.%, the interference effect discontinued and thus ΔT_{sol} shows a backward turning trend (Figure 4b/Table 2). Figure 4b displays the overall trends in average T_{lum} and ΔT_{sol} as functions of Tb doping level. It is interesting to find that 6 at.% Tb-doping is a turning point for both properties, at which average T_{lum} is at maximum while ΔT_{sol} is the lowest. It is worth noting that the phenomenal relative enhancement of T_{lum} of ~80% at 6 at.% doping level has surpassed the best reported dopings as shown in Table 1. From the data obtained, the overall best combination of thermochromic properties happens at 2 at.% Tb-doping, there is an obvious relative enhancement (~ 18%) in average T_{lum} compared to the undoped sample, while ΔT_{sol} is also increased slightly from 7.7% to 8.3%. The hysteresis loops of %T recorded at the wavelength of 2500nm were formed upon heating and cooling as depicted in Figure 4c, indicating that the MIT is a first order phase transition. The temperatures at which the sharpest changes happen in both heating and cooling curves are taken from the hysteresis loops as $\tau_{c, \text{ heating}} / \tau_{c, \text{ cooling}}$. The average of $\tau_{c, \text{ heating}}$ and $\tau_{c, \text{ cooling}}$ represents the τ_c , while the difference ($\Delta\tau_c = \tau_{c, \text{ heating}} - \tau_{c, \text{ cooling}}$) is the hysteresis loop width. As tabulated in Table 2, Tb-doping reduces τ_c at a rate of 1.5 °C/at.% up to 5 at.%, after which τ_c returns back to the value of undoped sample (67.5 °C) and even get higher to 72.5 °C at 8 at.% Tb-doping (Figure 4d). This might be explained by the competition between the effect of large ionic radius (increasing strain energy) and h^+ carrier density. In other words, the larger ionic radius of Tb^{3+} results in the τ_c reduction at lower doping level (< 5 at.%)³⁰ whilst the high concentration of h^+ carrier gives rise to the τ_c increment at higher doping level.³¹ The τ_c reduction

under Tb doping is in accordance with the density functional theory study on doped VO₂ materials with large radius cations.³² Compared with the reported F-,³³ Mg-,³⁴ Zr-doped or W-Zr-codoped VO₂ thin films,³⁵ the Tb doped VO₂ exhibits the largest T_{lum} but less ΔT_{sol} .

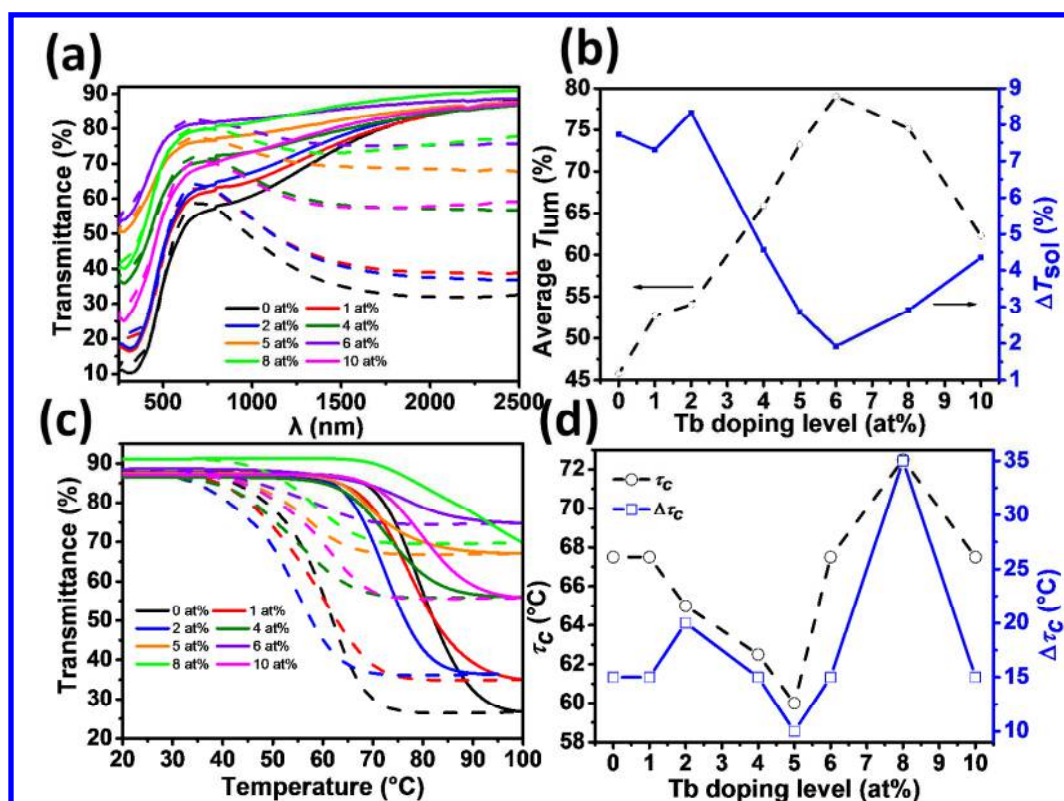


Figure 4. a) UV-Vis-NIR spectra of Tb-doped VO₂ thin films, all collected at 20 °C (solid lines) and 90 °C (dashed lines); b) Plots of doping level dependent average T_{lum} and ΔT_{sol} for Tb-doped VO₂ thin films; c) %T hysteresis loops of Tb-doped VO₂ thin films collected at $\lambda = 2500$ nm. Solid lines represent the heating processes and the dashed lines are the cooling curves; d) Phase transition temperatures (τ_c) and hysteresis loop width ($\Delta\tau_c$) of Tb-doped VO₂ thin films.

Table 2. Summary of experimental results for Tb-doped VO₂ thin films

Doping level (at.%)	Thickness (nm) ^{a)}	T_{lum} (%)		ΔT_{lum} (%)	T_{sol} (%)		ΔT_{sol} (%)	τ_c (°C)	$\Delta\tau_c$ (°C)	Grain size (nm) ^{b)}
		20 °C	90 °C		20 °C	90 °C				
		0	100	44.5	47.1	-2.6	51.6	43.9	7.7	
1	100	52.0	53.3	-1.3	57.1	49.8	7.3	67.5	15	60.0
2	100	53.4	54.7	-1.3	58.7	50.3	8.3	65.0	20	61.5
4	100	65.4	66.4	-1.0	68.1	63.5	4.6	62.5	15	71.0
5	100	72.8	73.6	-0.8	74.6	71.7	2.9	60.0	10	60.1
6	100	78.6	79.5	-0.9	79.4	77.5	1.9	67.5	15	57.5
8	100	74.8	75.4	-0.6	76.4	73.5	2.9	72.5	35	73.6
10	100	61.3	63.3	-2.0	65.4	61.1	4.4	67.5	15	97.8

^{a)} The thickness derivation is within 10 nm. ^{b)} The mean grain sizes were obtained from the respective AFM images.

3.3 Band gap of the thin films

As illustrated in literature,³⁶ the optical band gap of semiconductors could be determined according to the expression $(\alpha\hbar\omega)^m = A(\hbar\omega - E_g)$, where $m=1/2, 1/3, 2, 2/3$ represents the indirect-allowed, indirect-forbidden, direct-allowed and direct-forbidden optical transition, respectively. In addition, the energy gap detected by optical experiment is usually the direct band gap owing to the momentum conservation with low-excitation probability during the optical transition between two different symmetry points.³⁷ Therefore, we determined the direct band gap of the pristine and doped VO₂ samples by fitting the linear part of the curve $(\alpha\hbar\omega)^2$ versus $\hbar\omega$ (Figure

5a) with the expression $(\alpha\hbar\omega)^2 = A(\hbar\omega - E_g)$, where α is the absorption coefficient ($\alpha d = -\ln(T/1-R)$), A is a constant and $\hbar\omega$ is the photon energy. As depicted in Figure 5b, the E_g is widened steadily from 2.67 to 3.0 eV along with the Tb doping (below 6 at.%), which should benefit the increase of T_{lum} as seen in Table 2. Such similar behavior has also been reported in Mg^{2+} doped VO_2 thin films.³⁸⁻⁴¹ However, upon further increasing the Tb doping, the E_g begins to decay slightly, resulting in a moderately drop of T_{lum} , which may be ascribed to the competition between the strain energy and the h^+ carrier density introduced by the Tb^{3+} doping.

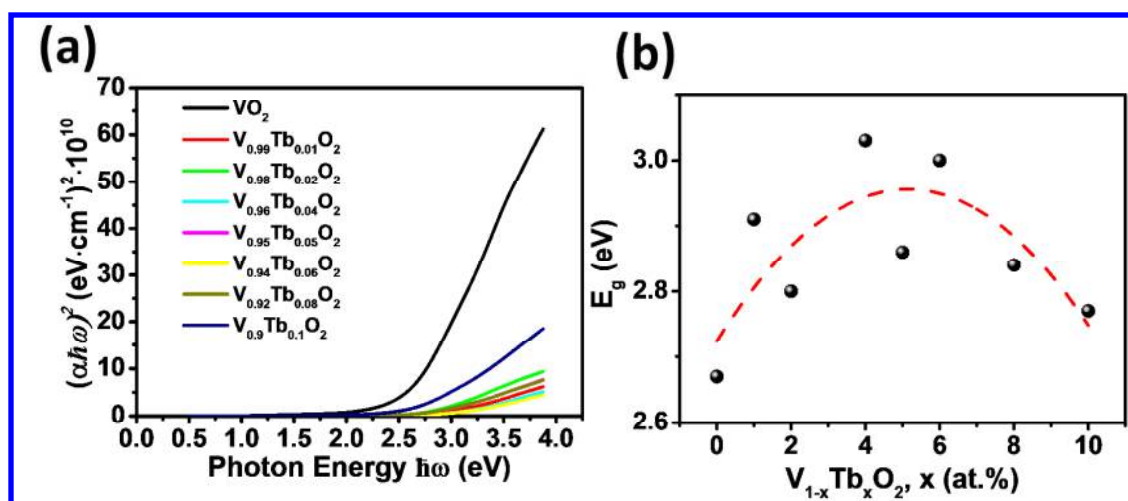


Figure 5. Plots of $(\alpha\hbar\omega)^2$ versus $\hbar\omega$ (a) and the photonic band gap E_g (b) of the VO_2 thin films.

Conclusions

In summary, the Tb^{3+} cations were firstly doped into the VO_2 lattice, and an enhancement of thermochromic properties in terms of reduced τ_c and largely increased T_{lum} was observed at the doping level from 1 at.% to 5 at.%. With Tb^{3+} doping from 1 at.% to 5 at.%, the T_{lum} was largely increased from 45.8% (pristine VO_2) to 73.2% while τ_c was marginally reduced from 67.5 °C (pristine VO_2) to 60 °C. However, upon further increasing the doping level to 10 at.%, the T_{lum}

1
2
3 was slightly depressed to 62.8% and the τ_c returned back to 67.5 °C, which should be mainly
4 ascribed to the competition between the strain energy and the free h^+ carrier density introduced
5 by the doping. With regard to the smart window applications, the future study on Tb-M (M=W,
6 Mg, F, Zr) –codoped VO₂ thin films may provide an alternative way to get a combination of high
7 T_{lum} as well as large ΔT_{sol} , considering the increase of T_{lum} with slightly compromised ΔT_{sol} in single Tb
8 doping.
9

18 AUTHOR INFORMATION

21 **Corresponding Author**

22 * Dr Yi Long. Email: longyi@ntu.edu.sg (Y. Long), Tel.: +65 67904599 Fax.: +65 67911604.
23

27 **Author Contributions**

28 The manuscript was written with contributions from all of the authors. All of the authors have
29 given approval to the final version of the manuscript.
30
31

35 **Acknowledgment**

36 This research is supported by the Singapore National Research Foundation under CREATE
37 programme: Nanomaterials for Energy and Water Management and Singapore Ministry of
38 Education (MOE) Academic Research Fund Tier 1 RG101/13 and an MSE-ERC Jülich
39 collaboration-MAP project grant. XRD, FESEM and TEM characterization was performed at the
40 Facility for Analysis, Characterization, Testing and Simulation (FACTS) in Nanyang
41 Technological University, Singapore and in the Ernst Ruska-Centre for Microscopy and
42 Spectroscopy with Electrons (ER-C) in Forschungszentrum Jülich, Germany. The authors
43 acknowledge financial support from the European Union under the Seventh Framework
44
45
46
47
48
49
50
51
52
53
54
55
56
57
58
59
60

1
2
3 Programme under a contract for an Integrated Infrastructure Initiative. Reference 312483 –
4
5 ESTEEM2. In addition, we thank Mr Min Hao Goh for XPS test.
6
7
8
9
10

11
12 References
13

- 14
15 1. Qazilbash, M. M.; Brehm, M.; Chae, B.-G.; Ho, P.-C.; Andreev, G. O.; Kim, B.-J.; Yun,
16
17 S. J.; Balatsky, A. V.; Maple, M. B.; Keilmann, F.; Kim, H.-T.; Basov, D. N. Mott
18
19 Transition in VO₂ Revealed by Infrared Spectroscopy and Nano-Imaging. *Science* **2007**,
20
21 318, 1750-1753.
22
23
- 24
25 2. Liu, M. K.; Hwang, H. Y.; Tao, H.; Strikwerda, A. C.; Fan, K. B.; Keiser, G. R.;
26
27 Sternbach, A. J.; West, K. G.; Kittiwatanakul, S.; Lu, J. W.; Wolf, S. A.; Omenetto, F.
28
29 G.; Zhang, X.; Nelson, K. A.; Averitt, R. D. Terahertz-field-induced insulator-to-metal
30
31 transition in vanadium dioxide metamaterial. *Nature* **2012**, 487, 345-348.
32
33
- 34
35 3. Zhou, Y.; Cai, Y.; Hu, X.; Long, Y. Temperature-responsive hydrogel with ultra-large
36
37 solar modulation and high luminous transmission for "smart window" applications. *J.*
38
39 *Mater. Chem. A* **2014**, 2, 13550-13555.
40
- 41
42 4. Zhou, Y.; Cai, Y.; Hu, X.; Long, Y. VO₂/hydrogel hybrid nanothermochromic material
43
44 with ultra-high solar modulation and luminous transmission. *J. Mater. Chem. A* **2015**, 3,
45
46 1121-1126.
47
- 48
49 5. Wang, N.; Magdassi, S.; Mandler, D.; Long, Y. Simple sol–gel process and one-step
50
51 annealing of vanadium dioxide thin films: Synthesis and thermochromic properties. *Thin*
52
53 *Solid Films* **2013**, 534, 594-598.
54
55
56
57
58
59
60

- 1
2
3
4
5
6
7
8
9
10
11
12
13
14
15
16
17
18
19
20
21
22
23
24
25
26
27
28
29
30
31
32
33
34
35
36
37
38
39
40
41
42
43
44
45
46
47
48
49
50
51
52
53
54
55
56
57
58
59
60
6. Wang, N.; Huang, Y.; Magdassi, S.; Mandler, D.; Liu, H.; Long, Y. Formation of VO₂ zero-dimensional/nanoporous layers with large supercooling effects and enhanced thermochromic properties. *RSC Adv.* **2013**, 3, 7124-7128.
7. Liu, C.; Wang, N.; Long, Y. Multifunctional overcoats on vanadium dioxide thermochromic thin films with enhanced luminous transmission and solar modulation, hydrophobicity and anti-oxidation. *Appl. Surf. Sci.* **2013**, 283, 222-226.
8. Boscolo, A.; Menosso, E.; Piuze, B.; Toppano, M. Thermochromic Materials for Temperature Sensors in New Applications. In *Device Applications of Nonlinear Dynamics*, Baglio, S.; Bulsara, A., Eds. Springer Berlin Heidelberg: **2006**; pp 139-144.
9. Jorgenson, G. V.; Lee, J. C. Doped vanadium oxide for optical switching films. *Solar Energy Materials* **1986**, 14, 205-214.
10. Chain, E. E. Optical properties of vanadium dioxide and vanadium pentoxide thin films. *Appl. Opt.* **1991**, 30, 2782-2787.
11. Chen, S.; Dai, L.; Liu, J.; Gao, Y.; Liu, X.; Chen, Z.; Zhou, J.; Cao, C.; Han, P.; Luo, H.; Kanahira, M. The visible transmittance and solar modulation ability of VO₂ flexible foils simultaneously improved by Ti doping: an optimization and first principle study. *Phys. Chem. Chem. Phys.* **2013**, 15, 17537-17543.
12. Strelcov, E.; Lilach, Y.; Kolmakov, A. Gas Sensor Based on Metal-Insulator Transition in VO₂ Nanowire Thermistor. *Nano Letters* **2009**, 9, 2322-2326.
13. Liu, C.; Cao, X.; Kamyshny, A.; Law, J. Y.; Magdassi, S.; Long, Y. VO₂/Si-Al gel nanocomposite thermochromic smart foils: Largely enhanced luminous transmittance and solar modulation. *J. Colloid Interface Sci.* **2014**, 427, 49-53.

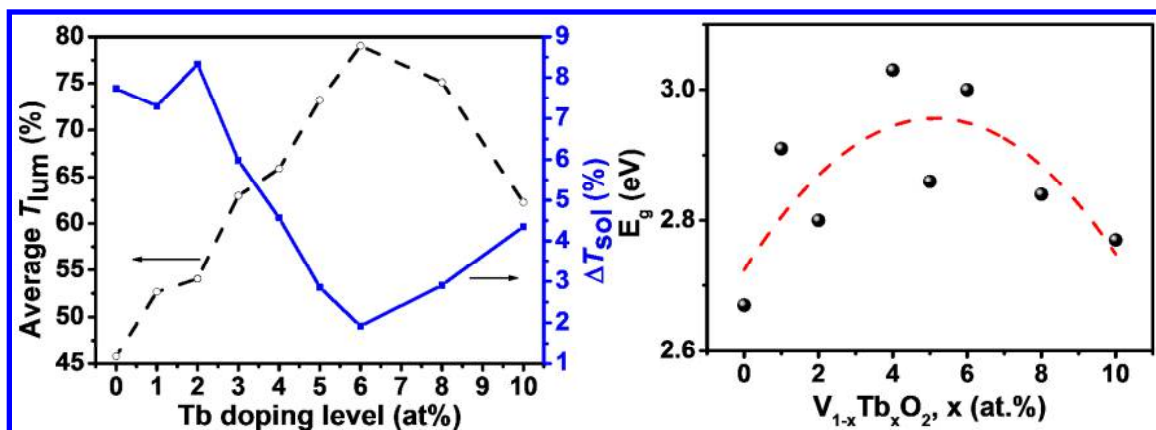
- 1
2
3
4
5
6
7
8
9
10
11
12
13
14
15
16
17
18
19
20
21
22
23
24
25
26
27
28
29
30
31
32
33
34
35
36
37
38
39
40
41
42
43
44
45
46
47
48
49
50
51
52
53
54
55
56
57
58
59
60
14. Chen, Z.; Gao, Y.; Kang, L.; Cao, C.; Chen, S.; Luo, H. Fine crystalline VO₂ nanoparticles: synthesis, abnormal phase transition temperatures and excellent optical properties of a derived VO₂ nanocomposite foil. *J. Mater. Chem. A* **2014**, *2*, 2718-2727.
 15. Qian, X.; Wang, N.; Li, Y.; Zhang, J.; Xu, Z.; Long, Y. Bioinspired Multifunctional Vanadium Dioxide: Improved Thermochromism and Hydrophobicity. *Langmuir* **2014**, *30*, 10766-10771.
 16. Cao, X.; Wang, N.; Law, J. Y.; Loo, S. C. J.; Magdassi, S.; Long, Y. Nanoporous Thermochromic VO₂ (M) Thin Films: Controlled Porosity, Largely Enhanced Luminous Transmittance and Solar Modulating Ability. *Langmuir* **2014**, *30*, 1710-1715.
 17. Cao, X.; Wang, N.; Magdassi, S.; Mandler, D.; Long, Y. Europium Doped Vanadium Dioxide Material: Reduced Phase Transition Temperature, Enhanced Luminous Transmittance and Solar Modulation. *Sci. Adv. Mater.* **2014**, *6*, 558-561.
 18. Mlyuka, N. R.; Niklasson, G. A.; Granqvist, C. G. Mg doping of thermochromic VO₂ films enhances the optical transmittance and decreases the metal-insulator transition temperature. *Appl. Phys. Lett.* **2009**, *95*, 171909.
 19. Li, S.-Y.; Niklasson, G. A.; Granqvist, C. G. Nanothermochromics: Calculations for VO₂ nanoparticles in dielectric hosts show much improved luminous transmittance and solar energy transmittance modulation. *J. Appl. Phys.* **2010**, *108*, 1-8.
 20. Li, S.-Y.; Niklasson, G. A.; Granqvist, C. G. Nanothermochromics with VO₂-based core-shell structures: Calculated luminous and solar optical properties. *J. Appl. Phys.* **2011**, *109*, 113515.

- 1
2
3
4
5
6
7
8
9
10
11
12
13
14
15
16
17
18
19
20
21
22
23
24
25
26
27
28
29
30
31
32
33
34
35
36
37
38
39
40
41
42
43
44
45
46
47
48
49
50
51
52
53
54
55
56
57
58
59
60
21. W.Burkhardt; T.Christmann; S.Franke; W.Kriegseis; D.Meister; B.K.Meyer; W.Niessner; D.Schalch; A.Scharmann. Tungsten and fluorine co-doping of VO₂ films. *Thin Solid Films* **2002**, 402, 226-231.
 22. Batista, C.; Ribeiro, R. M.; Teixeira, V. Synthesis and characterization of VO₂-based thermochromic thin films for energy-efficient windows. *Nanoscale Res. Lett.* **2011**, 6, 301.
 23. Ufert, K.-D. Doping of VO₂ Thin Films by Ion Implantation. *phys. stat. sol. (a)* **1977**, 42, 187-190.
 24. T. E. Phillips; R. A. Murphy; Poehler, T. O. Electrical Studies of Reactively Sputtered Fe-Doped VO₂ Thin Films. *Mat. Res. Bull.* **1987**, 22 1113-1123.
 25. Gao, Y.; Cao, C.; Dai, L.; Luo, H.; Kanehira, M.; Ding, Y.; Wang, Z. L. Phase and shape controlled VO₂ nanostructures by antimony doping. *Energy Environ. Sci.* **2012**, 5, 8708.
 26. Du, J.; Gao, Y.; Luo, H.; Zhang, Z.; Kang, L.; Chen, Z. Formation and metal-to-insulator transition properties of VO₂-ZrV₂O₇ composite films by polymer-assisted deposition. *Sol. Energy Mater. Sol. Cells* **2011**, 95, 1604-1609.
 27. Cao, J.; Ertekin, E.; Srinivasan, V.; Fan, W.; Huang, S.; Zheng, H.; Yim, J. W. L.; Khanal, D. R.; Ogletree, D. F.; Grossman, J. C.; Wu, J. Strain engineering and one-dimensional organization of metal-insulator domains in single-crystal vanadium dioxide beams. *Nat. Nanotechnol.* **2009**, 4, 732-737.
 28. Wyszecki G. and Stiles W. S. *Color Science: Concepts and Methods, Quantative Data and Fomulae*, Wiley, New York, Second edn., **2000**.

- 1
2
3
4
5
6
7
8
9
10
11
12
13
14
15
16
17
18
19
20
21
22
23
24
25
26
27
28
29
30
31
32
33
34
35
36
37
38
39
40
41
42
43
44
45
46
47
48
49
50
51
52
53
54
55
56
57
58
59
60
29. ASTM G173-03 Standard Tables of Reference Solar Spectral Irradiances: Direct Normal and Hemispherical on a 37° Tilted Surface, Annual Book of ASTM Standards American Society for Testing and Materials, Philadelphia, PA, USA, **2003**.
30. Kiri, P.; Hyett, G.; Binions, R. Solid state thermochromic materials. *Adv. Mater. Lett.* **2010**, 1, 86-105.
31. Goodenough, J. B. The Two Components of the Crystallographic Transition in VO₂. *J. Solid State Chem.* **1971**, 3, 490-500.
32. Sun, C.; Yan, L.; Yue, B.; Liu, H.; Gao, Y. The modulation of metal-insulator transition temperature of vanadium dioxide: a density functional theory study. *J. Mater. Chem. C* **2014**, 2, 9283-9293.
33. Dai, L.; Chen, S.; Liu, J.; Gao, Y.; Zhou, J.; Chen, Z.; Cao, C.; Luo, H.; Kanehira, M. F-doped VO₂ nanoparticles for thermochromic energy-saving foils with modified color and enhanced solar-heat shielding ability. *Phys. Chem. Chem. Phys.* **2013**, 15, 11723-11729.
34. Zhou, J.; Gao, Y.; Liu, X.; Chen, Z.; Dai, L.; Cao, C.; Luo, H.; Kanahira, M.; Sun, C.; Yan, L. Mg-doped VO₂ nanoparticles: hydrothermal synthesis, enhanced visible transmittance and decreased metal-insulator transition temperature. *Phys. Chem. Chem. Phys.* **2013**, 15, 7505-7511.
35. Shen, N.; Chen, S.; Chen, Z.; Liu, X.; Cao, C.; Dong, B.; Luo, H.; Liu, J.; Gao, Y. The synthesis and performance of Zr-doped and W-Zr-codoped VO₂ nanoparticles and derived flexible foils. *J. Mater. Chem. A* **2014**, 2, 15087-15093.
36. Tauc, J.; Menth, A. States in the gap. *J. Non-Cryst. Solids* **1972**, 8-10, 569-585.
37. Liu, G.-H.; Deng, X.-Y.; Wen, R. Electronic and optical properties of monoclinic and rutile vanadium dioxide. *J. Mater. Sci.* **2010**, 45, 3270-3275.

- 1
2
3
4
5
6
7
8
9
10
11
12
13
14
15
16
17
18
19
20
21
22
23
24
25
26
27
28
29
30
31
32
33
34
35
36
37
38
39
40
41
42
43
44
45
46
47
48
49
50
51
52
53
54
55
56
57
58
59
60
38. Li, S.-Y.; Mlyuka, N. R.; Primetzhofer, D.; Hallén, A.; Possnert, G.; Niklasson, G. A.; Granqvist, C. G. Bandgap widening in thermochromic Mg-doped VO₂ thin films: Quantitative data based on optical absorption. *Appl. Phys. Lett.* **2013**, 103, 161907.
39. Li, S. Y.; Niklasson, G. A.; Granqvist, C. G. Thermochromic fenestration with VO₂-based materials: Three challenges and how they can be met. *Thin Solid Films* **2012**, 520, 3823-3828.
40. Hu, S.; Li, S. Y.; Ahuja, R.; Granqvist, C. G.; Hermansson, K.; Niklasson, G. A.; Scheicher, R. H. Optical properties of Mg-doped VO₂: Absorption measurements and hybrid functional calculations. *Appl. Phys. Lett.* **2012**, 101, 201902.
41. Gagaoudakis, E.; Kortidis, I.; Michail, G.; Tsagaraki, K.; Binas, V.; Kiriakidis, G.; Aperathitis, E. Study of low temperature rf-sputtered Mg-doped vanadium dioxide thermochromic films deposited on low-emissivity substrates. *Thin Solid Films*, **2015**, In press.

Table of Contents Graphic and Synopsis



Series of Tb doped VO_2 thin films were prepared with a facile sol-gel method, which exhibited the largely enhanced (> 70%) visible transmission and widening optical bandgap below 6 at.% doping level.